Estimation of Fingertip Force Direction With Computer Vision

Yu Sun, *Member, IEEE*, John M. Hollerbach, *Fellow, IEEE*, and Stephen A. Mascaro, *Member, IEEE*

***Abstract*—This paper presents a method of imaging the coloration pattern in the fingernail and surrounding skin to infer fingertip force direction (which includes four major shear-force directions plus normal force) during planar contact. Nail images from 15 subjects were registered to reference images with random sample consensus (RANSAC) and then warped to an atlas with elastic registration. With linear discriminant analysis, common linear features corresponding to force directions, but irrelevant to subjects, are automatically extracted. The common feature regions in the fingernail and surrounding skin are consistent with observation and previous studies. Without any individual calibration, the overall recognition accuracy on test images of 15 subjects was 90%. With individual training, the overall recognition accuracy on test images of 15 subjects was 94%. The lowest imaging resolution, without sacrificing classification accuracy, was found to be between 10-by-10 and 20-by-20 pixels.**

***Index Terms*—Elastic registration, force sensing, haptic interfaces, human–computer interaction (HCI), linear discriminant analysis (LDA), random sample consensus (RANSAC).**

I. Introduction

THERE are myriad devices for manual input to a computer, such as keyboards, mice, touch pads, and force sticks [1]. One aspect of manual input is the exertion of fingertip force to control a cursor on a screen or to trigger an event, such as a key click. The detection of fingertip force in these contexts requires some form of external force sensor, such as arrayed capacitance sensors to detect the deflection of a membrane in a touch panel, or force sensors in the force stick of some laptop keyboards. These devices may be limited or unsuitable for use in certain applications and environments, as they may only work on certain surfaces and often cannot be reconfigured without reinstallation of hardware. They may be damaged in rough environments and may be activated by accidental contact with something other than a finger [16].

An alternative to force-based input devices is to employ computer-vision techniques, not only to track fingertip position [3], [5], [14], which can directly control a mouse cursor, but also to infer force events or force intents at the fingertip. Inferring fingertip force, such as mouse clicks or keyboard clicks, using only computer vision has proved problematical. Virtual keyboards have been proposed that project a keyboard image onto a plane [20]. One camera tracks each finger position, and another views a plane of light parallel to the projected surface and detects when a fingertip pierces this plane, which is interpreted as a key click. This approach requires multiple cameras and users to keep their hands suspended over the light plane, which may lead to fatigue. Approaches in [2], [4], and [6] required a finger to remain over a location for a certain amount of time so that the system could capture it as a click.

Rather than these indirect methods, which map finger kinematics into force, computer vision can measure the effect of contact force on the appearance of the fingertip. Kurita *et al.* [13] inferred contact force by observing tissue deformation at the point of contact. Fingerprints were imaged through a glass plate by a camera, and their deformation led to an estimate of the incipient slip movement between the fingertip and the glass. However, to generate detectable deformation and to prevent large sliding, the users had to apply a high force (around 10 N), which would be perceived as pressing very hard, and is near or above the limit of what can be exerted without getting fatigued [17]; typical grasp forces are much less, i.e., often below 5 N. Also, this method is obviously limited to situations where the fingertip can be imaged through a transparent surface.

A different approach was proposed by Mascaro and Asada [17], [18], who observed that the coloration pattern in the fingernail reflects the contact force state on the finger-pad. The blood perfusion underneath the fingernail is affected by the pressure at the finger-pad during contact with a surface due to the interaction between the fingernail, bone, and tissue. Fig. 1 qualitatively shows how different longitudinal shear forces (F_y is forward shear force, $-F_y$ is backward shear force, and $-F_z$ is the normal force) result in different regions of tension and compression in the skin. Compression squeezes out the blood, thus resulting in whitening, while tension pools the blood [19], which results in reddening.

Since humans have similar nail–bone–tissue structures, the effect of fingertip force on coloration is qualitatively similar

Manuscript received November 13, 2008; revised May 13, 2009 and August 25, 2009. First published November 10, 2009; current version published December 8, 2009. This paper was recommended for publication by Associate Editor H. R. Choi and Editor W. K. Chung upon evaluation of the reviewers' comments. This work was supported by the National Institutes of Health under Grant 1R21EB004600-01A2.

Y. Sun is with the Department of Computer Science and Engineering, University of South Florida, Tampa, FL 33620 USA (e-mail: yusun@cse.usf.edu).

J. M. Hollerbach is with the School of Computing, University of Utah, Salt Lake City, UT 84112 USA (e-mail: jmh@cs.utah.edu).

S. A. Mascaro is with the Department of Mechanical Engineering, University of Utah, Salt Lake City, UT 84112 USA (e-mail: smascaro@mech.utah.edu).

This paper has supplementary downloadable multimedia material available at http:/ieeexplore.ieee.org, provided by the author. This material includes two videos, namely, ImageDirection_demo1 and ImageDirection_demo2. ImageDirection_demo1 shows a computer game to use the fingertip force direction as the input to move a robot hand around in a cage to catch falling soccer balls. ImageDirection_demo2 shows an HCI application. A camera tracked a fingertip and detected if the fingertip pressed on a virtual button, and then a touch key activation was signaled by the fingernail of the virtual fingertip flashing white. The size is not specified. The contact for further questions about this work is gianluca@cs.umn.edu.

Color versions of one or more of the figures in this paper are available online at http://ieeexplore.ieee.org.

Digital Object Identifier 10.1109/TRO.2009.2032954

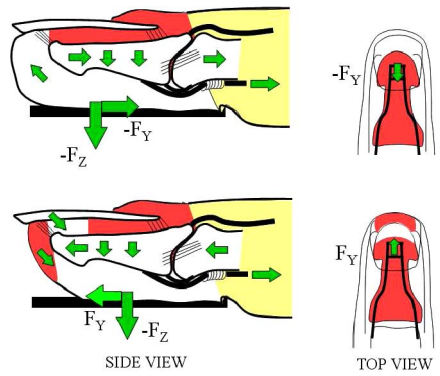

Fig. 1. Dark areas represent areas of tension where blood is pooled. The white area at the tip of the fingernail represents compression where blood is squeezed out.

across individuals. To demonstrate such commonality, Mascaro and Asada [18] imaged the fingernails of 16 subjects with a camera and deformed the fingernails to a standard circular shape by cropping, normalization according to the length and width of the fingernail, and pixel-by-pixel correlation. Defining the fingertip force as $F = [F_x, F_y, F_z]$, where $\pm F_x$ is lateral shear, they studied six different force states: zero force $= [0\ \ 0\ \ 0]$ N, normal force $= [0\ \ 0\ \ -3]$ N, left shear $= [-2\ \ 0\ \ -3]$ N, right shear $= [+2\ \ 0\ \ -3]$ N, backward shear $= [0\ \ -2\ \ -3]$ N, and forward shear $= [0\ \ 2\ \ -3]$ N. The same general color patterns were observed for all 16 subjects for each force state. Moreover, with one exception, the different force states yielded distinctly different coloration patterns. The exception was normal force and backward shear force, which had similar patterns of coloration.

For the most precise estimate of fingertip force, it is necessary to calibrate the coloration response to different force levels for each individual's fingernail. Mascaro and Asada [18] employed a six-axis force sensor and user-generated forces under guidance of a visual display and imaged the coloration response with a special visual sensor, which is termed as a photoplethysmograph (PPG). This sensor looks like an artificial nail and attaches to the back of the fingernail. The sensor was comprised of an array of six LED's for illumination and eight photodetectors embedded in an epoxy substrate and was custom-fabricated for each fingernail shape. In effect, it is a coarse camera with limited detection at a few predefined locations on the fingernail. Using different system-identification techniques, including least squares, their results showed very limited accuracy: a linear response to 1 N with an accuracy of 0.5 N and a saturation at 2 N.

The advantages of the PPG sensor are its portability and controlled lighting environment. The disadvantages are the need for individual fabrication and the limited sensing of the fingernail coloration pattern. More recently, we have employed external imaging of each fingernail with a video camera in order to avoid individual fabrication and to obtain a dense image not only of the fingernail but of the surrounding skin [24], [25] as well. Because of the dense images, a much higher accuracy of force prediction is obtained; in fact, the skin surrounding the fingernail also usefully indicates fingertip force, but the skin region was not imaged by the PPG. A linear response was obtained in [24] and [25] to 10 N (depending on the subject) with an accuracy of 0.5 N. Shear-force components, as well as the normal-force component could be estimated. These results pertain to fingertip contact on a flat surface and a flat finger-pad (nail roughly parallel to the surface). The coloration effect is also sensitive to surface curvature (edges and corners), as well as to different orientations of the finger-pad against the surface.

A difficulty with our previous work [24], [25] is the requirement for extensive individual calibration, which is suitable for the scientific study of grasp forces, but not for human–computer interaction (HCI). As far as possible, very little or no calibration should be required of a user in the field. This paper presents an atlas-based technique that meets this requirement. In the laboratory, fingertip force is precisely related to coloration for a number of subjects to build up an atlas of responses. Different fingernails are mapped by elastic registration into predefined shapes, and the common coloration features are extracted by linear discriminant analysis (LDA). In the field, the atlas is employed to quickly identify the force state of a new user's fingertip by relating the user's feature vectors to those of the atlas. This method sacrifices the prediction accuracy possible with individual calibration in favor of being able to predict six major force directions. This is sufficient to create an HCI that easily simulates the vertical input functionality of pressing buttons or keys, as well as the horizontal input functionality of a force stick that is presently limited to four discrete directions/inputs.

Based on their PPG sensor, Mascaro and Asada [16] proposed a "virtual switch" human–machine interface, where finger touch is detected and used to activate virtual switches located on any surface in the environment. The fingernail-imaging method, which is described in this paper, now augments the functionality of these virtual switches to create a virtual force-pad on any surface in view of a webcam, which can pick up the finger-pressing signal as well as shear-force direction signal, and use that signal to control a computer or a machine. Compared with traditional HCI approaches, this vision-based approach offers many advantages. It allows any flat surface to be used as a keyboard or as a touch pad. The surface can even be on a machine, such as a robot arm so that the human instructor can guide the robot's motion naturally. With a wearable camera, the HCI interface follows the user and is ready for interaction at any time and place. It is very suitable for virtual reality applications with a large workspace. Since the sensing mechanism is in the fingertip other than on the contact surface, the contact location is unlimited. It is not subject to wear and tear, like in the case of traditional sensors, and cannot be accidentally activated by contact with objects other than the finger. The setup of the interaction, such as keyboard layout, can be rearranged and reconfigured conveniently in software to reduce the cost for a system upgrade. In addition, this approach can be easily extended to involve multiple fingers to enrich the input freedom.

II. Laboratory Setup

The first step is building the feature atlas in a laboratory setting. Fig. 2 shows the experimental setup, which is comprised

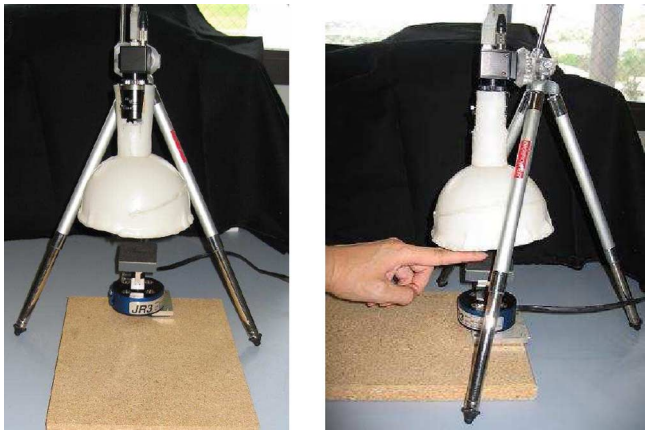

Fig. 2. Flea 2-D high-resolution camera images a contact plane, which is mounted on a six-axis JR3 force sensor through a lighting dome. Front and side views.

of a six-axis JR3 force sensor, a Flea charge-coupled device (CCD) video camera (Point Grey Research, Inc.), a tripod, and a small lighting dome. A rubber-surface flat plane is mounted on the JR3 force sensor to provide a contact surface. Subjects exert six directional forces on the JR3 force sensor: the four major shear-force directions, which are expressed by $\pm F_x$ and $\pm F_y$, normal force only, which is expressed by $-F_z$, and no force, which is expressed by F_{zero}.

The small lighting dome provides a controlled lighting environment so that the images taken at different times are comparable. A reflective hemisphere was created from molded plastic; a hole at the top permits visual access by the Flea camera. LEDs placed along the perimeter reflect off the dome to create uniform lighting on the fingernail surface and to avoid specular reflection.

Images are captured from the Flea camera at 30 frame per second (FPS), synchronously with recorded forces from the JR3 force sensor. In combination with the lens, the Flea camera measures an image that is about 8 cm along the optical axis and is about 4×3 cm in cross section. The green channel from the camera's Red, Green, and Blue (RGB) color space has been found to produce a larger coloration response and better linearity with force than the other color channels and is used subsequently.

We collected 20 images for each of the six force directions for 15 subjects that vary in age, size, sex, and race. All the autoadjustment functions of the camera were turned off so that the internal condition of the camera does not change over images.

A visual display (see Fig. 3) provides the indications of applied force to the subjects. Two of the three dimensions of force, which are read from the JR3 force sensor, are represented by position, while the third dimension is represented by the radius of a circle. Colors are used in the actual display. There is a blue circle with a blue cross in the center to represent the actual force applied, as measured by the JR3 force sensor beneath the finger. The x position of the cross represents lateral shear force, the y position represents longitudinal shear force, and the size of the circle represents the normal force.

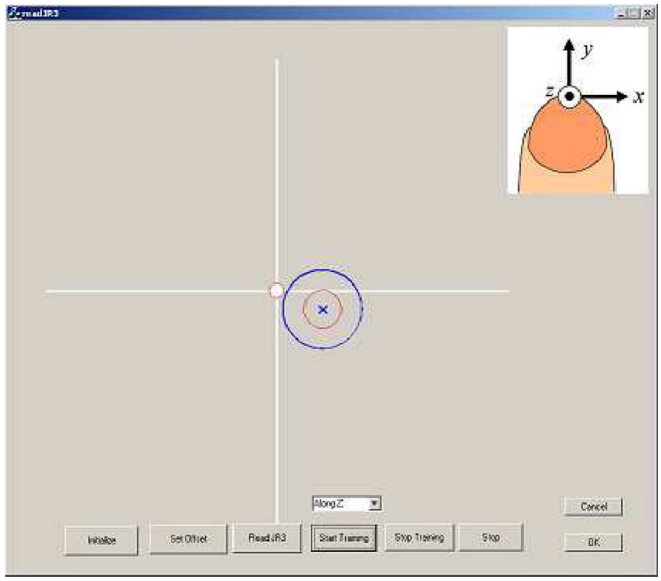

Fig. 3. Visual display feedback.

In contrast to [18], where distinct force amplitudes were specified, subjects were allowed to apply different levels of shear and normal force according to their comfort. For directional shear forces, the subjects needed to exert some normal force to prevent sliding. For zero force, the subjects were asked to rest their fingers on the force sensor to yield a small normal force. An example for 15 subjects is shown in Fig. 4. The lower boundary of the force in each direction is specified as 1.5 N. When the normal force is between 0 and -0.5 N, we view it as zero force. Subjects were asked to remove their fingers from the force sensor between recordings.

III. Finger-Image Registration

We assume that the distal phalanx is a rigid body, which is true when the observation is the back of the distal phalanx and the small deformation of the side skin can be ignored. When the distance between the finger and the camera is far larger than the curvature of the fingernail, we can assume that the surface of the fingernail and surrounding skin is planar.

To study the color pattern in the fingernail and surrounding skin in response to different fingertip force directions requires an analysis of images taken at different times. Finger posture varies over time relative to the camera. To compare the images, it is necessary to align them to avoid the orientation and position difference. We call the registration between images of one finger as intrafinger registration. Background subtraction is carried out for all images, as described in [26]. One zero-force image of each subject is selected to be the intrafinger reference image. In the experiment, the intrafinger reference images are taken with a standard orientation. All the other nail images for each subject are registered to the reference image.

To study the color pattern across the population, images of different fingers should be comparable. Meaningful regions, such as the distal, middle, and proximal zone, of the nail should

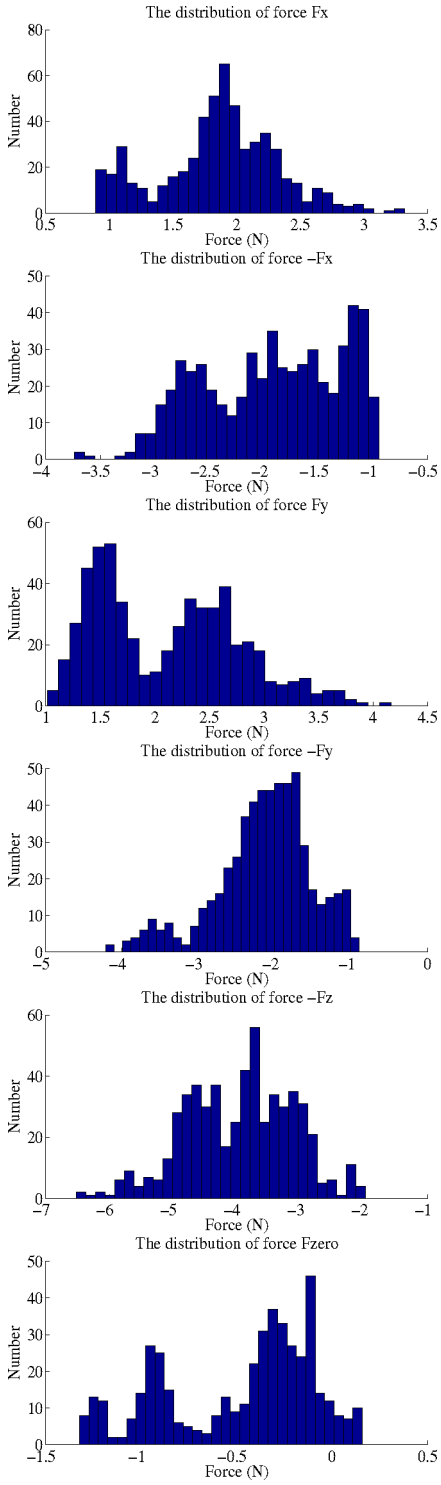

Fig. 4. Force distribution for six directions of 15 subjects

be consistent for different fingers. We call the registration of different fingers to an atlas finger as interfinger registration.

A. *Intrafinger Registration*

Since we assume that the surface of the fingernail and surrounding skin is a plane, the transformation between a point (x', y') in a new image and a point (x, y) in the reference image

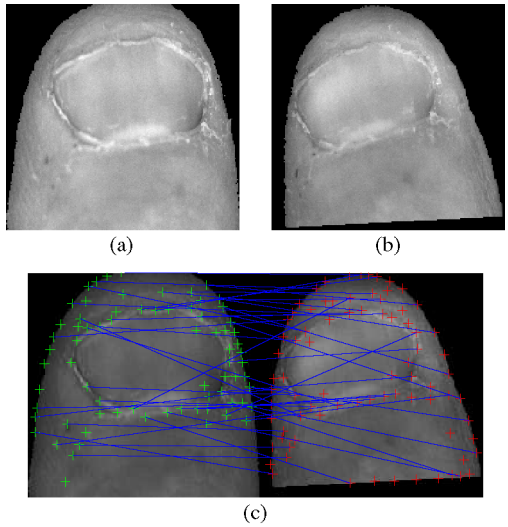

Fig. 5. (a) Reference image. (b) New image. (c) Feature points are marked as $+$'s in both images. The corresponding pairs, which are obtained with correlation, are connected with lines.

is a homography

$$\begin{bmatrix} x' \\ y' \\ 1 \end{bmatrix} = \mathbf{H} \begin{bmatrix} x \\ y \\ 1 \end{bmatrix}$$

where $\mathbf{H}$ is a 3×3 matrix. To determine the nine elements in $\mathbf{H}$ requires at least four correspondences in both images. The correspondences are automatically obtained with feature detection [12], correlation, and random sample consensus (RANSAC) [10], as follows.

1) Harris feature-point detection [12] is used to automatically detect feature points in both the new image [see Fig. 5(a)] and the reference image [see Fig. 5(b)], as shown in Fig. 5(c).
2) The detected feature points in two images are paired by examining pixel-intensity correlation within surrounding windows of the feature points. Only points that correlate most strongly with each other are paired. Fig. 5(c) shows the pairing by connecting the corresponding points with lines.
3) A 2-D homography mapping model is fitted robustly with RANSAC to select inliers, which are the correspondences [see Fig. 6(a)].

With the correspondences in the new image and the reference image, the 2-D homography can be calculated with least squares. With the homography matrix, the new image is then mapped to the reference image. Fig. 6(b) shows the transformation result. Fig. 6(c) shows the overlap of the transformation result and the reference image. We can see that they match well. With the same process, each new image of a finger is mapped to the reference image.

B. *Interfinger Registration*

A simplified shape for the fingertip is created for the atlas [see Fig. 7(f)]. The fingernail is modeled as a disk, and the

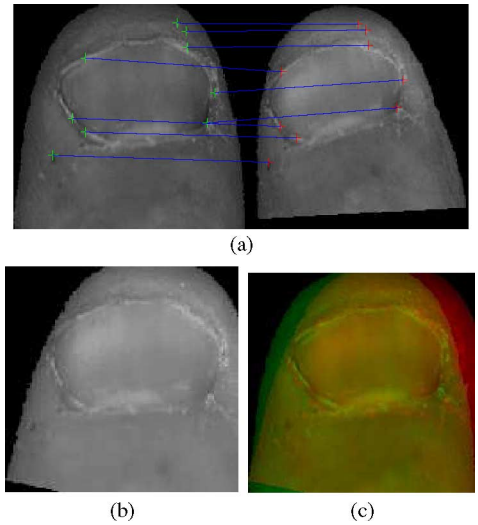

Fig. 6. (a) Correspondences after RANSAC. (b) Intrafinger registration result. (c) The registration result is overlayed on the reference image for comparison.

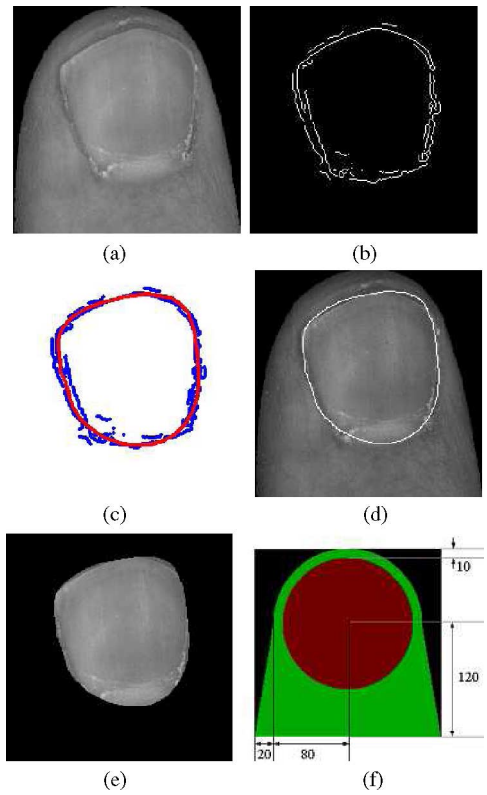

Fig. 7. (a) Finger image. (b) Canny-edge-detection result. (c) Cubic B-spline fits the edges. (d) Contour of the fingernail is shown as a white closed loop. (e) Region within the boundary is the fingernail. (f) Atlas of the full back of the fingertip. The fingernail is modeled as a disk with 70 pixels radius. The surrounding skin region is composed as a ring (70 pixels inner radius and 80 pixels outer radius) and an isosceles trapezoid (160 and 200 pixels for two bases, respectively).

surrounding skin region is composed of a ring and an isosceles trapezoid.

Ideally, the fingernails are mapped to the fingernail atlas, and the surrounding skin is mapped to the surrounding skin atlas.

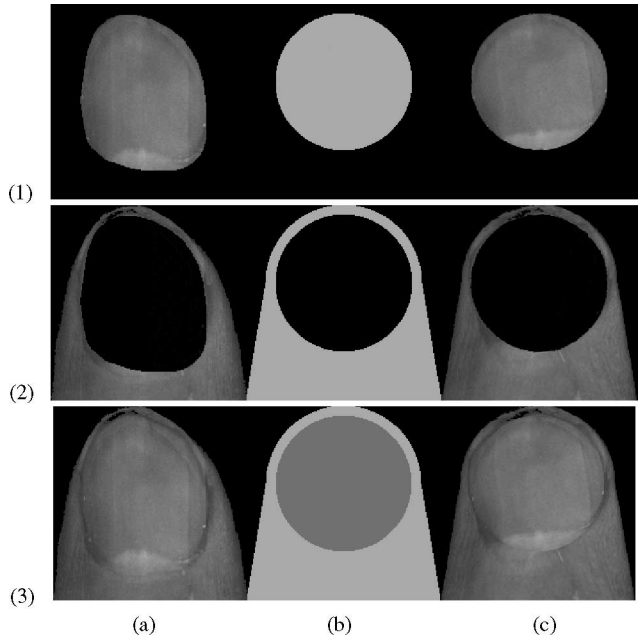

Fig. 8. Rows 1–3 are the segmented fingernail, the surrounding skin, and the whole finger. (a) Original image. (b) Atlas shape. (c) Elastic warping result.

To do so, fingernails in the reference images need to be segmented from the surrounding skin. We use a Canny edge filter to automatically detect the boundary of the fingernail. Because of the broken skin around the fingernail, the automatically detected boundary is noisy and rarely forms a smooth curve. The edge-detection result of a typical finger [see Fig. 7(a)] is shown in Fig. 7(b). We use cubic B-splines to fit the edges and achieve a close-loop contour, as shown in Fig. 7(c). The region inside of the contour is the segmented nail, as shown in Fig. 7(e).

The nail and the surrounding skin can be transformed to the atlas image, respectively, with boundary-based elastic-deformation transformation [8], [21]. We model both the fingernail and surrounding skin regions as elastic sheets that are warped by an external force field applied to the boundaries. Since elastic warping tends to preserve color-pattern shapes and the relative position of the patterns, it is well-suited for color-pattern comparison across subjects.

We assume that both the fingernail boundary and surrounding skin boundary can be homotopically transformed to the defined boundary in the atlas image. The boundaries in an image are first deformed into their corresponding boundaries in the atlas. The mapping of the rest of the images is calculated by solving the equations that describe the deformation of an elastic sheet with the boundary deformations. Detailed description can be found in [8] and [21] with different elastic models. With the elastic deformation model, the pixel-to-pixel mapping can be calculated. With a cubic interpolation for pixel values, the finger image can be deformed to the atlas image.

The interfinger registration process is illustrated in Fig. 8. After the fingernail and surrounding skin are registered, respectively (see rows (1) and (2) of Fig. 8), the registration results are combined to generate the registration of the whole finger

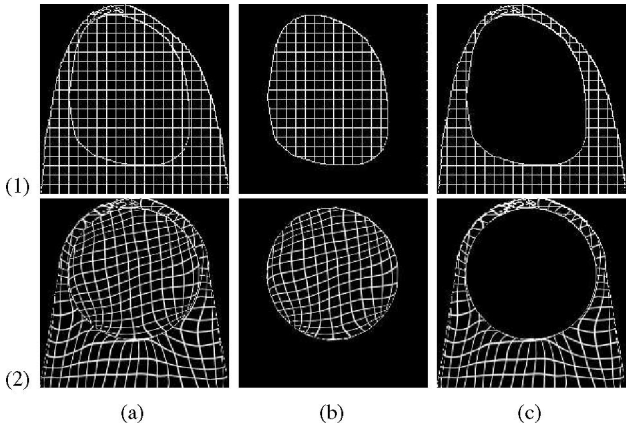

Fig. 9. Deformation mapping shown with grids. Row 1 shows the source images, and row 2 shows the target deformation mapping. The deformation mapping of the whole image, the nail, and the skin are displayed in columns (a)–(c), respectively.

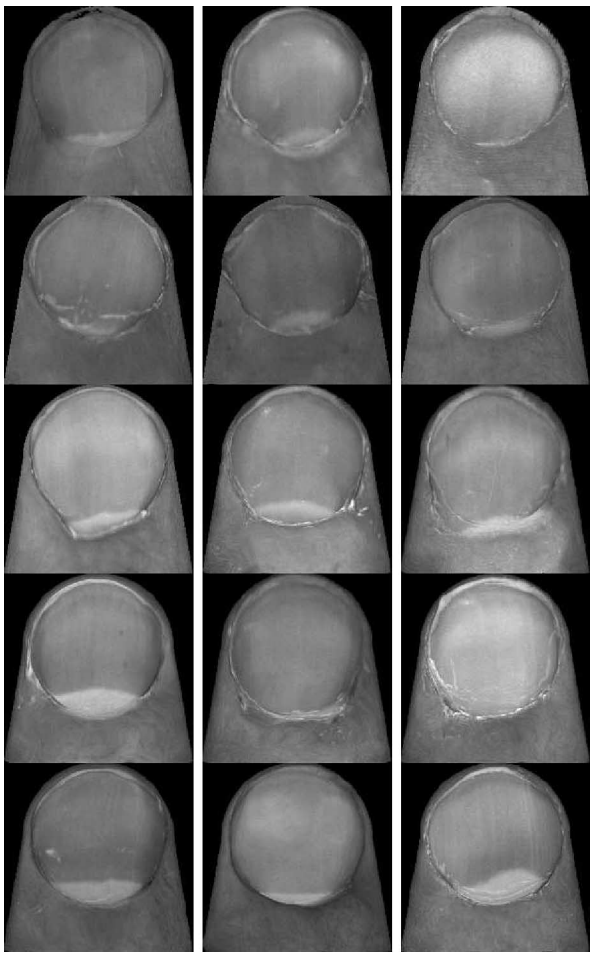

Fig. 10. Elastic registration result for all 15 subjects.

image [see row (3) of Fig. 8]. The deformation mappings are illustrated in Fig. 9 with grids.

The interfinger registration results for all the 15 subjects are shown in Fig. 10; the original images are shown in Fig. 11. The registration results preserve color-pattern shapes and the relative position of the patterns.

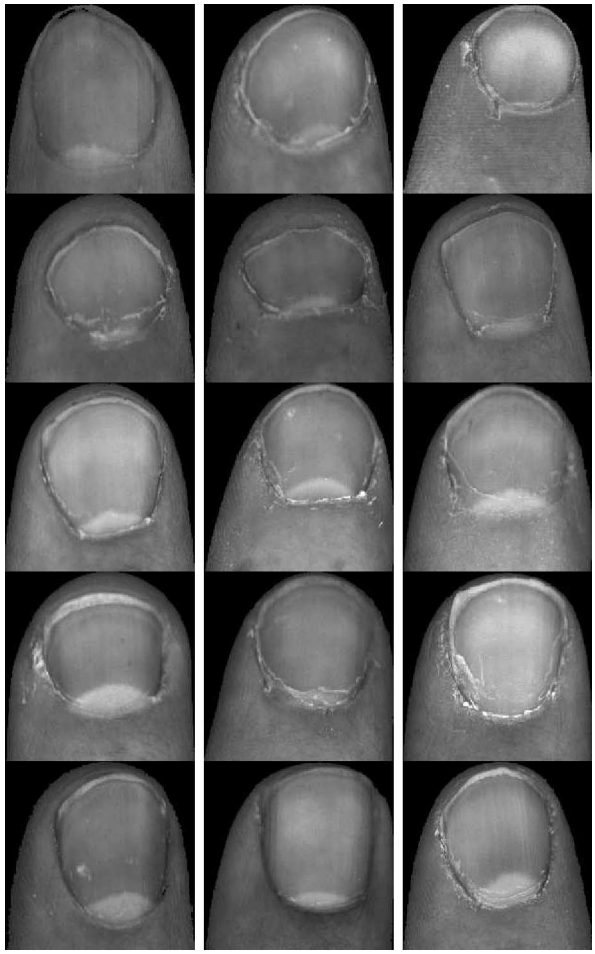

Fig. 11. Source images for all 15 subjects before warping.

IV. Color-Pattern Identification

As discovered in [18], [24], and [25], with different directions of force applied on the fingertip, the color patterns in the fingernail and surrounding skin are different. The different color patterns can be used to classify the finger images to six classes corresponding to six force directions. Since the color patterns in the images are very high dimensional, we need a feature-extraction method to find low-dimensional features to best describe the color patterns. Since applications of this technique usually requires low latency, a linear feature extraction is preferred [15]. Moreover, because we are seeking common color-pattern features for all people and all force levels (see Fig. 4), the extracted feature should not only maximize the differences between the six classes but also minimize the variation between subjects and the variation caused by different force levels. The well-known LDA [7], [11] is a good match.

A. Linear Discriminant Analysis Features Extraction

For an $N \times N$ fingernail with skin image, the pixels are recast as an N^2-dimensional vector $\mathbf{I}$. For class $\mathcal{D}_i$ of the C classes, there are M_i training vectors. The definitions of the between-class scatter matrix $\mathbf{S}_B$ and within-class scatter matrix

$\mathbf{S}_W$ are

$$\mathbf{S}_B = \sum_{i=1}^{C} M_i(\mathbf{m}_i - \mathbf{m})(\mathbf{m}_i - \mathbf{m})^T \quad (1)$$

$$\mathbf{S}_W = \sum_{i=1}^{C} \sum_{\mathbf{I}\in\mathcal{D}_i} (\mathbf{I} - \mathbf{m}_i)(\mathbf{I} - \mathbf{m}_i)^T \quad (2)$$

where $\mathbf{m}_i$ is the mean vector for class $\mathcal{D}_i$, and $\mathbf{m}$ is the total mean vector, with

$$\mathbf{m}_i = \frac{1}{M_i} \sum_{\mathbf{I}\in\mathcal{D}_i} \mathbf{I} \quad (3)$$

$$\mathbf{m} = \frac{\sum_{i=1}^{C} M_i \mathbf{m}_i}{\sum_{i=1}^{C} M_i}. \quad (4)$$

The feature-extraction problem is the same as to find projection vectors $\mathbf{W}$ that maximize the ratio of the between-class scatter matrix $\mathbf{S}_B$ to the within-class scatter matrix $\mathbf{S}_W$

$$\mathbf{J}(\mathbf{W}) = \frac{|\mathbf{W}^T \mathbf{S}_B \mathbf{W}|}{|\mathbf{W}^T \mathbf{S}_W \mathbf{W}|}. \quad (5)$$

This is the same as

$$\mathbf{J}'(\mathbf{W}) = \frac{|\mathbf{W}^T \mathbf{S}_B \mathbf{W}|}{|\mathbf{W}^T \mathbf{S}_T \mathbf{W}|} \quad (6)$$

where $\mathbf{S}_T = \mathbf{S}_W + \mathbf{S}_B$ is the scatter matrix of the entire data. Finding the vectors to maximize $\mathbf{J}'(\cdot)$ is a generalized eigenproblem. The columns of an optimal $\mathbf{W}$ are the $C-1$ generalized eigenvectors of

$$\mathbf{S}_B \mathbf{w}_i = \lambda_i \mathbf{S}_T \mathbf{w}_i \quad (7)$$

where C is the number of classes; here, $C = 6$. Since $\mathbf{S}_T$ is always singular when the number of training data is smaller than the dimension of the data, a principal component analysis (PCA) is used to reduce the dimension [7]. This process is usually referred to as PCA–LDA. As studied in [27], the performance of the PCA–LDA approach heavily depends on the selections of principal components (PCs) in the PCA step. We use a PCA-selection scheme, which is based on the correlation between the PCs of $\mathbf{S}_T$ and the PCs of $\mathbf{S}_B$ [27].

B. Features

A total of 1800 training images with corresponding force directions obtained from the force sensor were taken for six force directions of 15 subjects: lateral shear-force directions, which are represented by F_x and $-F_x$, longitudinal shear-force directions, which are represented by F_y and $-F_y$, normal force, which is represented by only $-F_z$, and no force, which is represented by F_{zero}. They were resized to 50×50 and labeled. All images were registered to their reference images and then to the atlas. With LDA, the linear feature vectors were extracted and illustrated in Fig. 12. The pixel values are the weights from feature vectors, which can be positive or negative. Since it is difficult to show negative pixels in an image, for one feature vector, we show the positive elements in one image and the absolute value of negative elements in another and call it the negative feature image. Columns (a) and (b) show the positive and negative feature images, respectively; columns (c) and (d) show just the fingernail area.

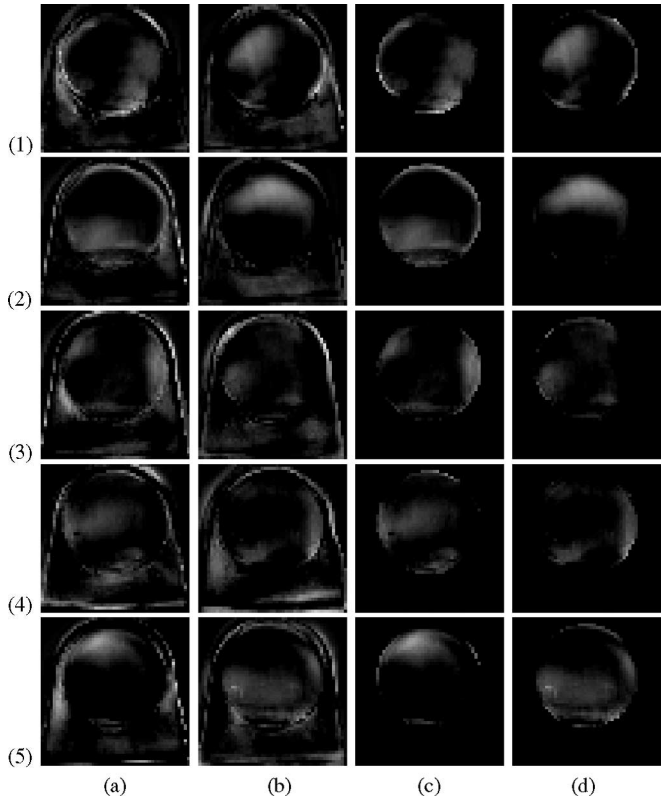

Fig. 12. Five linear discriminant features for 15 subjects. (a) Positive features of the fingernail and surrounding skin. (b) Negative features of the fingernail and surrounding skin. To understand better, (c) and (d) show the positive features and negative features in the fingernail only.

The highlights in the distal and middle of the nail atlas are consistent with previous observations: the white zones observed in [17] and [18] and the best-response regions in [24] and [25]. The feature regions in the second row have been explained as the interaction between tissue, nail, and bone [17]. The other highlighted regions in the feature images are the left-distal, left-proximal, right-distal, and right-proximal portions of the nail, respectively. This is consistent with previous observations, but previously, not much was done with these particular observations. These results may also be valuable for the mechanical study of the nail–bone–tissue interaction. Other than the nail, the surrounding skin also has useful feature regions. The feature areas in the surrounding skin not only reflect the color change pattern but also show the deformation of the skin.

The feature regions, which are shown in Fig. 12, do not explicitly illustrate which color pattern corresponds to which force direction. The means of the groups in the feature space represent the common color pattern disregarding the individual differences. The reconstructed images of the means are displayed in Fig. 13.

The differences are too small to be seen. For better observation, the mean image of group F_{zero} is subtracted from the mean images of groups F_x, $-F_x$, F_y, $-F_y$, and $-F_z$. The

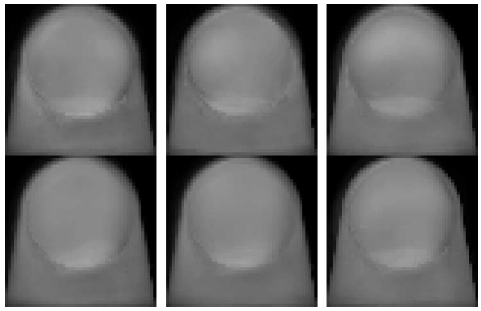

Fig. 13. Means images of each groups projected on the 5-D feature space. From top-left to bottom-right are means images of groups F_x, $-F_x$, F_y, $-F_y$, $-F_z$, and F_{zero}.

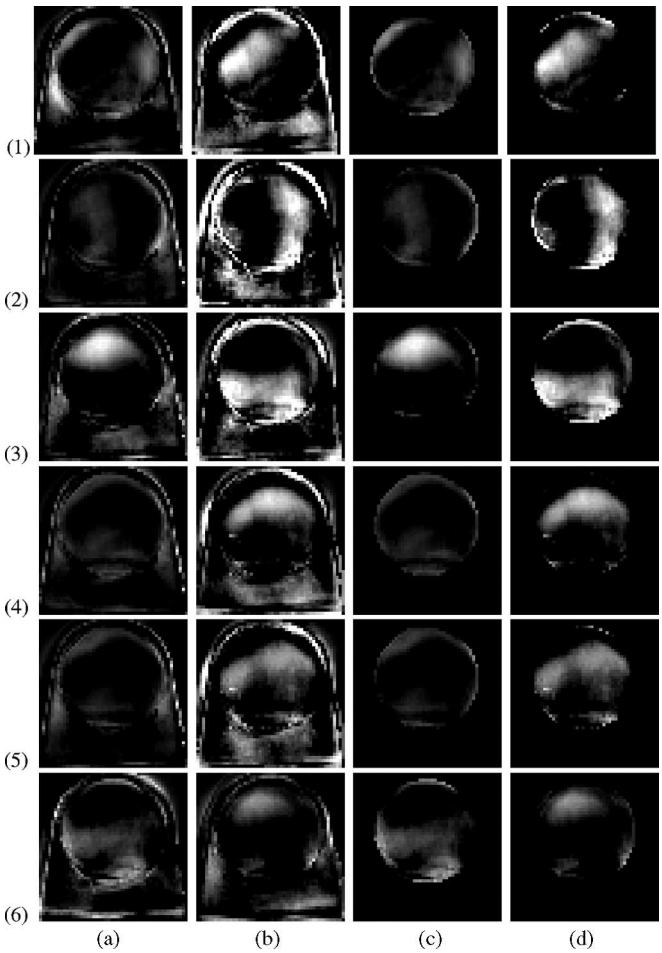

Fig. 14. [Rows (1)–(5)] Differences between the mean images of groups F_x, $-F_x$, F_y, $-F_y$, and $-F_z$, and the mean image of group F_{zero}, respectively. [Row (6)] Mean image of group $-F_y$ subtracted from the mean image of group $-F_z$. (a) Positive differences. (b) Negative differences. The fingernail is isolated in (c) and (d), corresponding to (a) and (b), respectively.

positive differences are scaled to the full scale of the pixel range 0–255, and are shown in rows (1)–(5) of Fig. 14. Row (6) shows the differences between the mean of groups *y* and *z*. The positive and negative differences are shown in columns (a) and (b), respectively. Columns (c) and (d) show just the fingernail area.

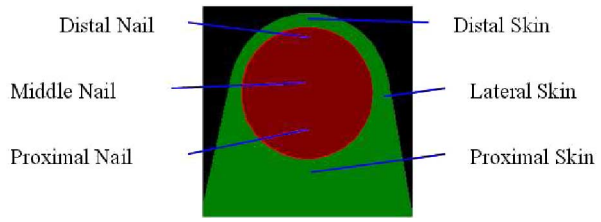

Fig. 15. Terminologies of the regions in the atlas of the fingernail and surrounding skin.

Fig. 15 illustrates the terminologies of the regions in the atlas. The color patterns in the fingernail can increase or decrease in gray scale, which corresponds to the color changing to white or dark red in color. The color patterns in the skin can come from the color change and the skin deformation. Skin disappearing can result in color decrease, since the background is zero and *vice versa*. From the difference images, which are shown in Fig. 14, the following conclusions are reached.

1) For shear-force direction F_x (see row (1) of Fig. 14), the common coloration response is a whitening of the left distal nail, the right middle nail, and the left lateral skin and a reddening of the left middle nail and the proximal skin.
2) For shear-force direction $-F_x$ (see row (2) of Fig. 14), there is a whitening of the left middle/proximal nail and the right lateral skin and a reddening of the right middle/proximal nail and the left proximal skin. The left upper lateral skin deforms and disappears.
3) For shear-force direction F_y (see row (3) of Fig. 14), there is a whitening of the upper middle nail and both sides of lateral skin and a reddening of the distal nail and proximal nail. The distal skin disappears.
4) For shear-force direction $-F_y$ (see row (4) of Fig. 14), there is a whitening of the distal and proximal nail and the side lateral skin and a reddening of the upper middle nail and the proximal skin.
5) For the normal-force direction $-F_z$ (see row (5) of Fig. 14), there is a whitening of the distal nail and the lateral skin and a reddening of the upper middle nail and the proximal skin.
6) The color pattern for $-F_y$ is very close to $-F_z$. From row (6) of Fig. 14, we found that the proximal nail whitens more for the $-F_y$ direction, while the distal nail reddens more. Because of deformation, more distal skin appears for $-F_y$ than for $-F_z$.

Since the color patterns are automatically extracted from all 15 subjects, and the feature-extraction method, namely, LDA, minimizes the different between subjects and emphasizes the difference caused by different force directions, the color patterns, which are described earlier, are the common color patterns for different force directions for all 15 subjects, disregarding the differences between subjects.

V. Classification

The feature space is 5-D. Fig. 16 shows the training data in the 2-D space spanned with the first two feature vectors. We can see

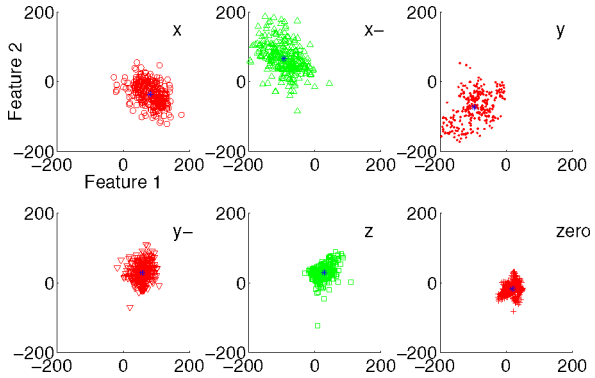

Fig. 16. Training images from 15 subjects are projected onto the plane spanned by the first two feature vectors. Images belonging to the same groups are displayed in a plot.

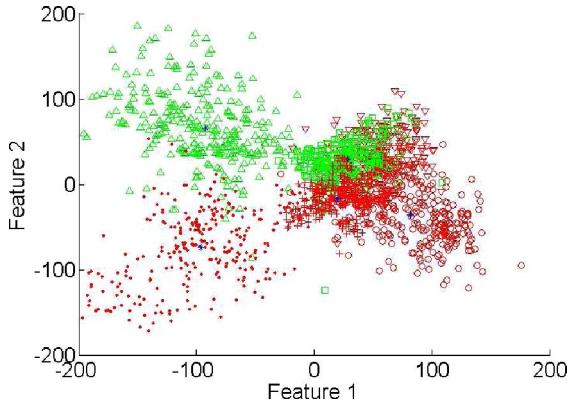

Fig. 17. Training images are projected on the plane spanned with the first two feature vectors. Six clusters represent the lateral shear-force directions $+F_x$ (which is denoted by $\circ$'s) and $-F_x$ (which is denoted by Δ's), the longitudinal shear-force directions $+F_y$ (which is denoted by $\cdot$'s) and $-F_y$ (which is denoted by ∇'s), normal force $-F_z$ only (which is denoted by $\square$'s), and no force (denoted by $+$'s).

that it is reasonable to assume the distributions of the clusters are multivariate normal. Therefore, for class ω_i, the distribution of an image $\mathbf{x}$ is

$$p(\mathbf{x}|\omega_i) \sim \mathcal{N}(\boldsymbol{\mu}_i, \boldsymbol{\Sigma}_i).$$

For group i, the means $\boldsymbol{\mu}_i$, and the covariance matrix $\boldsymbol{\Sigma}_i$ are unknown. With the labeled training images, they can be estimated with maximum likelihood

$$\hat{\boldsymbol{\mu}}_i = \frac{1}{n_i}\sum_{k=1}^{n_i}\mathbf{x}_{ik}$$

and

$$\hat{\boldsymbol{\Sigma}}_i = \frac{1}{n_i}\sum_{k=1}^{n_i}(\mathbf{x}_{ik}-\hat{\boldsymbol{\mu}}_i)(\mathbf{x}_{ik}-\hat{\boldsymbol{\mu}}_i)^T$$

where n_i is the training image number in group i.

The training images from Fig. 16 are combined in Fig. 17. With just two feature vectors, images with $+F_x$, $-F_x$, $+F_y$, and F_{zero} are seen to be well separable. However, the color patterns of the $-F_z$ and $-F_y$-directional forces are too similar to distinguish without further steps.

TABLE I
ACCURACY RESULTS FOR EACH OF 15 SUBJECTS

Subject	All	$-F_{z,y}$	No $-F_y$
1	78%	90%	98%
2	93%	99%	100%
3	95%	97%	91%
4	84%	99%	100%
5	95%	100%	100%
6	88%	92%	92%
7	91%	97%	98%
8	86%	98%	100%
8	92%	94%	95%
10	99%	100%	97%
11	83%	88%	80%
12	86%	98%	97%
13	94%	94%	96%
14	99%	100%	100%
15	87%	98%	97%
Total	90%	96%	96%

A. *Bayesian Classifier*

Recognition is made in a 5-D space spanned by the feature vectors. In order to achieve minimum-error rate, the classifier is

$$g_i(\mathbf{x}) = P(\omega_i|\mathbf{x}) = \frac{1}{C}p(\mathbf{x}|\omega_i)P(\omega_i)$$

for a test image $\mathbf{x}$, where C is a normalization constant, and ω denotes the state of class. It assigns a test image $\mathbf{x}$ to class ω_i if

$$g_i(\mathbf{x}) > g_j(\mathbf{x}), \qquad \text{for all } j \neq i.$$

Taking the natural logarithm, we have

$$g_i(\mathbf{x}) = \ln p(\mathbf{x}|\omega_i) + \ln P(\omega_i).$$

We assume that the priors are equal for all classes. The likelihoods are learned from training data, and they are multinormal, which is given by $p(\mathbf{x}|\omega_i) \sim \mathcal{N}(\boldsymbol{\mu}, \boldsymbol{\Sigma}_i)$. Thus, the classifier is

$$g_i(\mathbf{x}) = -\frac{1}{2}(\mathbf{x}-\boldsymbol{\mu}_i)^T\boldsymbol{\Sigma}_i^{-1}(\mathbf{x}-\boldsymbol{\mu}_i) - \frac{d}{2}\ln 2\pi - \frac{1}{2}\ln|\boldsymbol{\Sigma}_i|.$$

New images are projected to the feature space and classified.

The recognition results for 1518 test images of six force directions for 15 subjects are shown in Table I. The overall accuracy is 90% with all directions in consideration [see column (2) of Table I], 96% by combining $-F_y$ and $-F_z$ into a single group [see column (3)], and 96% without including $-F_y$ [see column (4) of Table I]. For all force directions, 8 out of 15 subjects have more than 90% accuracy. Two subjects have a 99% accuracy.

In terms of accuracy by force direction, Table II shows that they are at least 95% except for $-F_y$ whose accuracy is around 79% (see column (2) "All" of Table II). Around 80% of misclassified $-F_y$ instances are classified in group $-F_z$. If the $-F_y$ and $-F_z$ are grouped together, then the accuracies are very close to perfect (see column (2) "$-F_{z/y}$" of Table II). Column (4), i.e., "No $-F_y$," again shows that accuracies are improved over column (2), i.e., "$-F_{z/y}$," by omitting the $-F_y$ group.

TABLE II
ACCURACY RESULTS FOR ALL SUBJECTS BY FORCE DIRECTION

Force	All	$-F_{z/y}$	No $-F_y$
F_x	98%	98%	99%
$-F_x$	98%	98%	97%
F_y	95%	95%	89%
$-F_y$	79%	94%	–
$-F_z$	79%	99%	98%
F_{zero}	96%	96%	98%
Total	90%	96%	96%

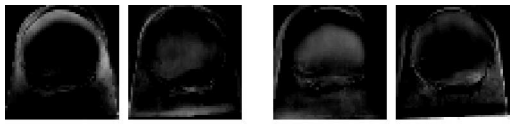

(a) (b)

Fig. 18. Two linear discriminant features for 15 subjects. (a) Positive features. (b) Negative features.

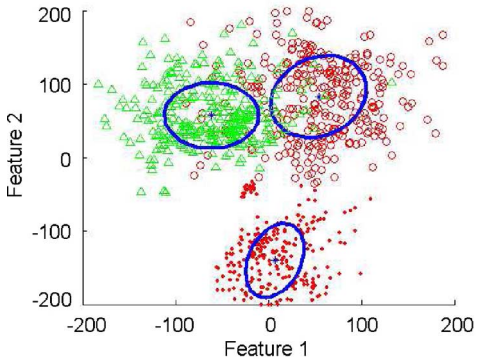

Fig. 19. Training images are projected on the plane spanned with the two feature vectors. Three clusters represent group $-F_y$ (denoted by $\circ$), group $-F_z$ (denoted by $\triangle$'s), and group $F_{\rm zero}$ (denoted by $\cdot$'s). The centers of clusters are indicated with $*$'s, and the variances are indicated with ellipses.

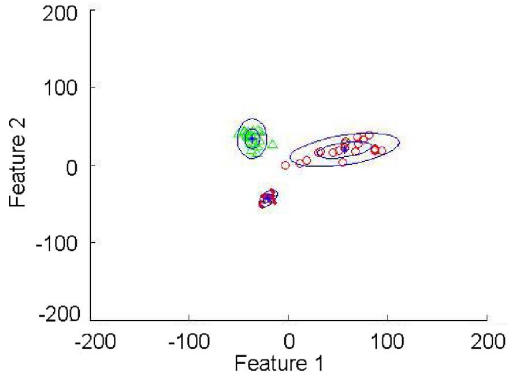

Fig. 20. Distributions of training groups $-F_y$, $-F_z$, and $F_{\rm zero}$ for one subject.

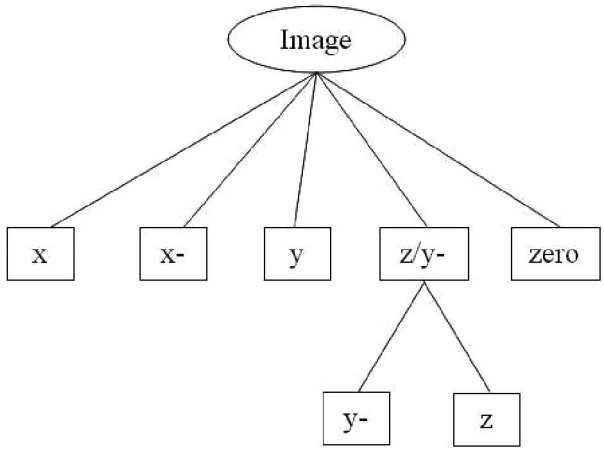

Fig. 21. Structure of the hierarchical classifier. The classification for the top layer is made with common features and common distributions. For the second layer, the distinction of $-F_y$ from $-F_z$ is made with individually trained distributions.

B. Distinction of $-F_z$ and $-F_y$

The recognition result in Table II indicates that there are around 40% of the images of the $-F_z$ and $-F_y$ directions that are not separable. Nevertheless, there are some differences in the images. LDA feature extraction was applied to image groups $-F_y$, $-F_z$, and $F_{\rm zero}$ while ignoring the other groups. Since the class number $C = 3$, therefore, the feature number is 2. The features trained with all 15 subjects are displayed in Fig. 18. The highlighted regions correspond to color patterns that responds to $-F_y$ and $-F_z$ directional force; visual observation agrees with this result.

The training images are projected into the 2-D feature space, as shown in Fig. 19. Clearly, groups $-F_y$ and $-F_z$ can be easily separated from group $F_{\rm zero}$ along feature 2. The majority of groups $-F_y$ and $-F_z$ can also be clearly separated, but small portions of training data could not be separated linearly. The means of the three groups are relatively distinct. The group $-F_z$ mean is to the left of the group $-F_y$ mean along feature 1.

To achieve better separation, the training distributions of each individual subject are inspected. For example, for subject 1, the distribution of groups $-F_z$, $-F_y$, and $F_{\rm zero}$ are plotted in Fig. 20. The training images for this subject can be well-separated when considered alone.

As shown in Table I, more than half of the subjects have overall accuracy more than 90%. For them, classification can be carried out with common distributions. For subjects with lower classification accuracy and particularly having low accuracy due to overwhelming differences between individuals, the distributions of $-F_y$ and $-F_z$ need to be trained individually.

C. Hierarchical Classifier

A hierarchical classifier is designed to combine the classification based on common distribution of groups F_x, $-F_x$, F_y, and $F_{\rm zero}$ and the classification based on individual distribution of groups $-F_y$ and $-F_z$, as shown in Fig. 21.

For a test image, the classifier first decides which category it belongs to with common distributions. If it belongs to group F_x, $-F_x$, F_y, or $F_{\rm zero}$, the classifier stops. Otherwise, the classification continues with individually trained distributions of $-F_y$ and $-F_z$. For the first layer, training is carried out with all subjects. For the second layer, training is carried out for each individual. Distributions learned for individuals are stored and

TABLE III
HIERARCHICAL VERSUS BAYESIAN CLASSIFIER FOR 15 SUBJECTS

Subject	Bayesian	Hierarchical
1	78%	84%
2	93%	94%
3	95%	95%
4	84%	90%
5	95%	95%
6	88%	98%
7	91%	95%
8	86%	90%
8	92%	94%
10	99%	98%
11	83%	88%
12	86%	95%
13	94%	94%
14	99%	99%
15	87%	98%
Total	90%	94%

TABLE IV
HIERARCHICAL VERSUS BAYESIAN CLASSIFIER BY FORCE DIRECTION

Force	Bayesian	Hierarchical
F_x	98%	98%
$-F_x$	98%	98%
F_y	95%	94%
$-F_y$	79%	87%
$-F_z$	79%	92%
F_{zero}	96%	96%
Total	90%	94%

used after the subject is identified as in [22]. The feature vectors used in both layers are commonly trained.

Table III shows the recognition accuracies of 1518 verification images for 15 subjects of the commonly trained Bayesian classifier [see columns (2)–(4) of Table III] versus the individually trained hierarchical classifier [see column (5) of Table III]. The overall accuracy of the hierarchical classifier is 94%, with a 4% increase. A total of 13 subjects are equal to or are more than 90% accurate; one subject has 88% accuracy, and one subject has 84% accuracy. Table IV shows the results by force direction for all subjects combined. The accuracies for $-F_y$ and $-F_z$ increased by 8% and 13%, respectively.

VI. RESOLUTION

The results show that a low-dimensional feature space can express the color patterns efficiently. This suggests that a high-resolution image is not necessary. In order to determine what the lowest resolution image might be that still gives good results, the image resolution was gradually increased from 2-by-2 pixels. The feature extracting, distribution learning, and classification are carried out after each resolution increment. The increment step is 1-by-1 pixel. As shown in Fig. 22, the overall accuracy increases rapidly from 0% to 87% before the resolution reaches 10-by-10 pixels. Thereafter, the accuracy increases slowly and oscillates. At 20-by-20 pixels, the accuracy reaches 93%. For the next 30 iterations, the accuracy increases only 1%.

Fig. 23 shows the feature images when the image size is 10-by-10, 20-by-20, and 50-by-50 pixels. The feature images of 20-by-20 pixels contain all the feature areas as that of the feature images of 50-by-50 pixels. For all subjects and directions, the 20-by-20 pixel resolution is the lowest resolution that

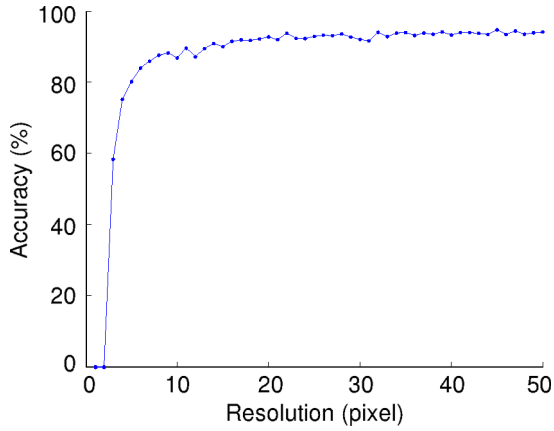

Fig. 22. Relation between the overall accuracy for all subjects and the resolution of the fingernail and surrounding skin. The row and column of the images are equal. The x-axis shows the row/column resolution.

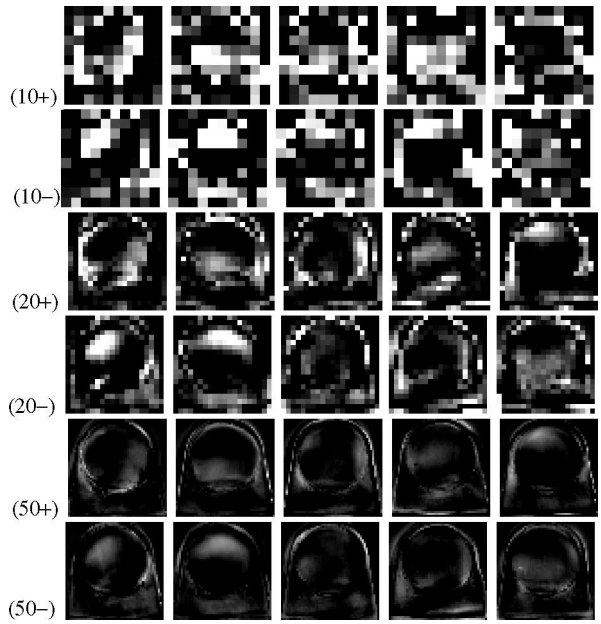

Fig. 23. Feature images corresponding to different resolutions. The plus and minus rows correspond to positive and negative features, respectively.

is still sufficient for force direction recognition. Therefore, this approach can be used with a low-resolution camera, such as a webcam, which also allows the capture of force directions of multiple fingers with one camera.

VII. DEMONSTRATION

To demonstrate the usage of the fingertip force direction, we have designed a computer game to use the fingertip force direction as the input to move a robot hand around in a cage to catch falling soccer balls. A video camera is used to monitor the color pattern in the fingernail and surrounding skin, and then, the color patterns are used to estimate fingertip force directions. The computer uses the fingertip force direction to move the robot hand around to catch falling soccer balls (see Fig. 24). This is like the force touch on some laptop keyboards. A short demo

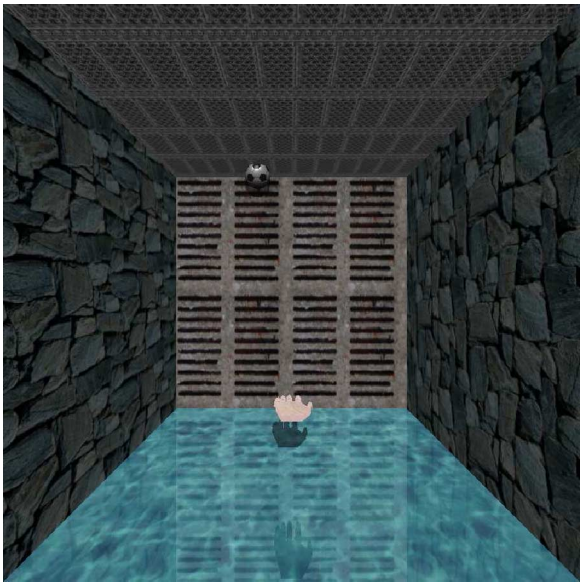

Fig. 24. Game that uses fingertip force direction as the input to move a robot hand around in order to catch falling soccer balls.

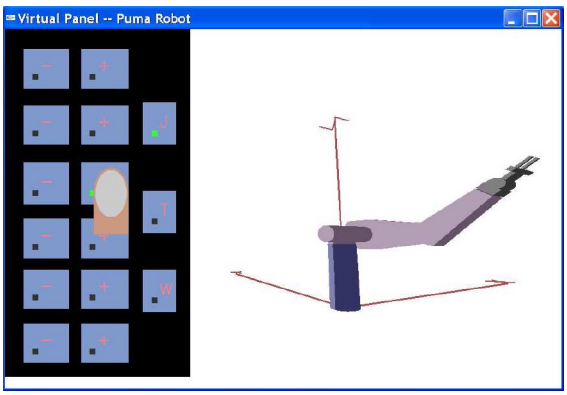

Fig. 25. Simulated programmable universal machine for assembly (PUMA) control panel pressed by a virtual finger.

video, in which a user plays this game with his index finger, is available with this paper as support material.

The technique, which is presented in this paper, can also replace keyboard or control panels to simulate a key click- or a touch-panel press. As shown in column (4) of Table II, where $-F_z$ is distinguished from F_{zero} with a 98% accuracy without any calibration, it is extremely easy and robust to recognize finger pressing by just looking at the fingernail. This means that any surface can become a control surface as long as it is visible by a camera. In combination with a visual display on a computer, any layout of touch-panel keys can be simulated. The virtual touch panel can be conveniently placed on a desk surface, on a kitchen counter, and at the side of a bed. In one example, we simulated the touch panel to control a PUMA robot, where a simulated fingertip also appeared on the visual display (see Fig. 25). A touch-key activation was signaled by the fingernail of the virtual fingertip flashing white. The effect could be reinforced by adding an audio display. A short video that demonstrates the control-panel approach is available with this paper as support material.

VIII. Discussion

This paper has investigated whether the fingernail coloration effect is suitable for HCI applications, as a substitute for touch panels, keyboards, and force sticks. These applications only require binary-force recognition. For touch-panel or key presses, only the normal force, which is expressed by $-F_z$, has to be distinguished from no force, which is expressed by F_{zero}. For the force-stick applications, all six force directions have to be distinguished in order to move the cursor up and down or left and right. To be practical in the field, there should be a reasonably high recognition accuracy and little or no individual calibration.

To get the highest accuracy of fingertip force estimation, time-consuming individual calibration is required [24], [25], which while suitable for scientific studies of grasping is not feasible for HCI. The approach that we have taken to avoid individual calibration is to build a common atlas of calibrated response properties in the laboratory for a number of individuals and then to apply this atlas to new users in the field. Although we cannot get accurate predictions of force levels using just the atlas, we are able to predict binary-force direction: longitudinal and lateral shear forces, which are denoted by $\pm F_y$ and $\pm F_x$, respectively, normal force only, which is denoted by $-F_z$, and no force, which is denoted by F_{zero}.

To build the atlas, the calibration results for different individuals have to be combined by registering their fingernail positions to a reference position (which is called intrafinger registration) and then warping to a simplified atlas shape (which is called interfinger registration). Intrafinger registration is achieved by Harris feature detection and RANSAC. Interfinger registration is achieved by segmenting the fingernail from the surrounding skin and then warping both to the atlas shapes using elastic registration.

To minimize the variance between subjects and the variance of force levels in each direction, LDA is applied to yield a 5-D feature space for image classification. A Bayesian classifier trained on the atlas was able to classify test images with an overall accuracy of 90%, but directions $\pm F_x$, F_y, and F_{zero} were classified with a much higher accuracy (more than 95%) than directions $-F_y$ and $-F_z$ (around 79%). Although the majority of $-F_y$ and $-F_z$ images are correctly classified, the coloration patterns are similar enough so that the differences between individuals overwhelms the differences for a single individual.

To achieve higher recognition accuracy, a small degree of individual training is required. A two-layer hierarchical classifier was designed, which includes individual training on the second layer. Images that are classified to $-F_y$ or $-F_z$ are further classified based on individually trained distributions of groups y and z. The accuracies for $-F_y$ and $-F_z$ increase to 87% and 92%, respectively, while the overall accuracy for all directions increases to 94%.

To simulate a force stick, the coloration effect's success is more qualified. Without individual calibration and use of the atlas only, most force directions are recognized with high accuracy, but $-F_z$ is not as easily distinguished from $-F_y$. Table I shows that for most subjects, the recognition accuracy is above 90% for these two directions, but a sizable minority of subjects

have recognition accuracies roughly between 80% and 90%. For such individuals, some amount of individual calibration is required. We are currently investigating whether simpler field-based calibration actions can be employed to disambiguate $-F_y$ from $-F_z$ for such subjects, rather than laboratory-based calibration. Specifically, in the case of the force stick, a pure normal force, which is denoted by $-F_z$, does not have a function. A classification of $-F_z$ as $-F_y$ may be a usable interpretation by a user. If a key click were to be implemented with the virtual force stick, however, they would have to be disambiguated.

This method currently is limited to recognizing six color patterns due to orthogonal forces. We found that the color pattern in the fingernail and surrounding skin changes continuously with the changes in force direction. Since our method is based on linear feature extraction, the continuity property remains in the LDA feature space. In demonstration, the diagonal movement was implemented with combination of x and y movement. In the future, we will investigate the possibility of integrating this technique with the force estimation in [24] and [25] to predict 3-D force continuously with little calibration.

The low-dimensional space for the recognition suggests that low image resolution may yield as good a result as high resolution. We found that the resolution can be as low as 10-by-10 pixels for reasonable accuracy, such as 87%, and 20-by-20 pixels for a higher accuracy of 93%, which means that low-cost and low-resolution cameras, such as a webcam, can be employed and that multiple fingers can be viewed with just one camera.

Currently, we have limited the fingertip orientation to lie flat on a surface, which we regard as a reasonable constraint on the user. We are able to detect whether the fingertip is at an unacceptable orientation and signal the user to that effect. The dependence of the coloration effect on fingertip orientation is a subject of future research.

Our experiments were carried out in controlled lighting conditions. However, since the LDA, which is a feature-extraction approach, is known to be insensitive to lighting changes, our approach would work the same in general lighting environment after more thorough training. The touch panel example shown in Fig. 25 has been demonstrated to work well in the lighting environment of a poster-display room in a conference with around 50 participants. All the participants could utilize the virtual control panel easily and comfortably.

ACKNOWLEDGMENT

Portions of this research have been published in [23].

REFERENCES

[1] S. K. Card, W. K. English, and B. J. Burr, "Evaluation of mouse, rate-controlled joystick, step keys, and text keys for text selection on a CRT," *Ergonom.*, vol. 21, pp. 601–613, 1978.

[2] X. Chen, H. Koike, Y. Nakanishi, and Y. Sato, "Two-handed drawing on augmented desk system," in *Proc. Int. Conf. Adv. Visual Interfaces*, May 2002, pp. 760–761.

[3] J. Crowley, J. Berard, and J. Coutaz, "Finger tracking as an input device for augmented reality," in *Proc. Int. Workshop Gesture Face Recognit.*, Zurich, Switzerland, Jun.1995, pp. 195–200.

[4] N. Takao, J. Shi, and S. Baker, "Tele-graffiti: A camera-projector based remote sketching system with hand-based user interface and automatic session summarization," *Int. J. Comput. Vis.*, vol. 53, pp. 115–133, 2003.

[5] P. Wellner, "Interacting with paper on the DigitalDesk," *Commun. ACM*, vol. 36, no. 7, pp. 86–97, 1993.

[6] Z. Zhang, "Visual panel: Virtual mouse keyboard and 3d controller with an ordinary piece of paper," in *Proc. Workshop Perceptive User Interfaces*. New York: ACM, Nov. 2001.

[7] P. N. Belhumeur, J. P. Hespanha, and D. J. Kriegman, "Eigenfaces vs. fisherfaces: Recognition using class specific linear projection," *IEEE Trans. Pattern Anal. Mach. Intell.*, vol. 19, no. 7, pp. 711–720, Jul. 1997.

[8] C. A. Davatzikos, R. N. Bryan, and J. L. Prince, "Image registration based on boundary mapping," *IEEE Trans. Med. Imag.*, vol. 15, no. 1, pp. 112–115, Feb. 1996.

[9] R. O. Duda, P. E. Hart, and D. G. Stork, *Pattern Classification*, 2nd ed. New York: Wiley, 2001.

[10] M. A. Fischler and R. C. Bolles, "Random sample consensus: A paradigm for model fitting with applications to image analysis and automated cartography," *Commun. Assoc. Comp.*, vol. 14, pp. 381–395, 1981.

[11] R. A. Fisher, "The statistical utilization of multiple measurements," *Ann. Eugen.*, vol. 8, pp. 376–386, 1938.

[12] C. G. Harris and M. J. Stephens, "A combined corner and edge detector," in *Proc. 4th Alvey Vis. Conf.*, 1988, pp. 147–151.

[13] Y. Kurita, A. Ikeda, J. Ueda, and T. Ogasawara, "A fingerprint pointing device utilizing the deformation of the fingertip during the incipient slip," *IEEE Trans. Robot.*, vol. 21, no. 5, pp. 801–811, Oct. 2005.

[14] J. Letessier and F. Berard, "Visual tracking of bare fingers for interactive surfaces," in *Proc. ACM Symp. User Interface Softw. Technol.*, 2004, pp. 119–122.

[15] A. M. Martinez and M. Zhu, "Where are linear feature extraction methods applicable?" *IEEE Trans. Pattern Anal. Mach. Intell.*, vol. 27, no. 12, pp. 1934–1944, Dec. 2005.

[16] S. A. Mascaro and H. H. Asada, "Virtual switch human–machine interface using fingernail touch sensors," in *Proc. IEEE Int. Conf. Robot. Autom.*, 1999, vol. 4, pp. 2533–2538.

[17] S. A. Mascaro and H. H. Asada, "Photoplethysmograph fingernail sensors for measuring finger forces without haptic obstruction," *IEEE Trans. Robot. Autom.*, vol. 17, no. 15, pp. 698–708, Oct. 2001.

[18] S. A. Mascaro and H. H. Asada, "Measurement of finger posture and three-axis fingertip touch force using fingernail sensors," *IEEE Trans. Robot. Autom.*, vol. 20, no. 1, pp. 26–35, Feb. 2004.

[19] S. A. Mascaro and H. H. Asada, "The common patterns of blood perfusion in the fingernail bed subject to fingertip touch force and finger posture," *Haptics-e*, vol. 4, no. 3, pp. 1–6, 2006.

[20] G. D. Morrison, "A camera-based input device for large interactive displays," *IEEE Comput. Graph. Appl.*, vol. 25, no. 4, pp. 52–57, Jul./Aug. 2005.

[21] S. Periaswamy and H. Farid, "Elastic registration in the presence of intensity variations," *IEEE Trans. Med. Imag.*, vol. 22, no. 7, pp. 865–874, Jul. 2003.

[22] Y. Sun, J. M. Hollerbach, and S. A. Mascaro, "Finger force direction recognition by principal component analysis of fingernail coloration pattern," in *Proc. World Haptics Conf.*, 2007, pp. 90–95.

[23] Y. Sun, J. M. Hollerbach, and S. A. Mascaro, "Imaging the fingertip force direction," in *Proc. IEEE Comput. Soc. Conf. Comput. Vis. Pattern Recognit.*, Minneapolis, MN, Jun. 18–23, 2007, pp. 1–6.

[24] Y. Sun, J. M. Hollerbach, and S. A. Mascaro, "Predicting fingertip forces by imaging coloration changes in the fingernail and surrounding Skin," *IEEE Trans. Biomed. Eng.*, vol. 55, no. 10, pp. 2363–2371, Oct. 2008.

[25] Y. Sun, J. M. Hollerbach, and S. A. Mascaro, "Measuring fingertip forces by imaging the fingernail," in *Proc. 14th Symp. Haptic Interfaces Virtual Environ. Teleoperator Syst.*, 2006, pp. 125–131.

[26] Y. Sun, J. M. Hollerbach, and S. A. Mascaro, "EigenNail for finger force direction recognition," in *Proc. IEEE Int. Conf. Robot. Autom.*, 2007, pp. 3251–3256.

[27] M. Zhu and A. M. Martinez, "Selecting principal components in a two-stage LDA algorithm," in *Proc. IEEE Comput. Soc. Conf. Comput. Vis. Pattern Recognit.*, 2006, pp. 132–137.

[28] W. T. Freeman, D. Anderson, P. Beardsley, C. Dodge, H. Kage, K. Kyuma, Y. Miyake, M. Roth, K. Tanaka, C. Weissman, and W. Yerazunis, "Computer vision for interactive computer graphics," *IEEE Comput. Graph. Appl.*, vol. 18, no. 3, pp. 42–53, May/Jun. 1998.

[29] F. Quek, T. Mysliwiec, and M. Zhao, "Finger mouse: A freehand pointing interface," in *Proc. Int. Workshop Autom. Face Gesture Comput. Recognit.*, 1995, pp. 372–377.

Yu Sun (S'03–M'07) received the B.S. and M.S. degrees in electrical engineering from the Dalian University of Technology, Dalian, China, in 1997 and 2000, respectively, and the Ph.D. degree in computer science from the University of Utah, Salt Lake City, in 2007.

He is currently an Assistant Professor with the Department of Computer Science and Engineering, University of South Florida, Tampa. From December 2007 to May 2008, he was a Postdoctoral Associate with Mitsubishi Electric Research Laboratories, Cambridge, MA. From May 2008 to May 2009, he was a Postdoctoral Associate with the School of Computing, University of Utah. His current research interests include robotics, computer vision, and haptics.

John M. Hollerbach (M'85–SM'92–F'96) received the B.S. degree in chemistry and the M.S. degree in mathematics from the University of Michigan, Ann Arbor, in 1968 and 1969, respectively, and the S.M. and Ph.D. degrees in computer science from the Massachusetts Institute of Technology (MIT), Cambridge, in 1975 and 1978, respectively.

He is currently a Professor with the School of Computing, University of Utah, Salt Lake City, where he directs the Robotics Track, as well as a Research Professor in mechanical engineering. From 1989 to 1994, he was the Natural Sciences and Engineering/Canadian Institute for Advanced Research Professor of robotics with the Departments of Mechanical Engineering and Biomedical Engineering, McGill University, Montreal, QC, Canada. From 1978 to 1982, he was a Research Scientist. From 1982 to 1989, he was a Faculty member with the Department of Brain and Cognitive Sciences and a member of the Artificial Intelligence Laboratory, MIT. He is currently an Editor of the *International Journal of Robotics Research*. His current research interests include robotics, virtual reality, and human motor control.

Dr. Hollerbach received the National Science Foundation Presidential Young Investigator Award in 1984, and in 1988, he was named a Fellow of the Canadian Institute for Advanced Research. He was the Program Chairman of the 1989 IEEE International Conference on Robotics and Automation. From 1989 to 1993, he was a member of the Administrative Committee of the IEEE Robotics and Automation Society. From 1989 to 1994, he was a Technical Editor of the IEEE TRANSACTIONS ON ROBOTICS AND AUTOMATION. He is currently the Vice President for Conference Activities of the IEEE Robotics and Automation Society.

Stephen A. Mascaro (S'97–M'03) received the B.A. degree in physics from Houghton College, Houghton, NY, in 1995, the B.S. degree in mechanical engineering from Clarkson University, Potsdam, NY, in 1995, and the M.S. and Ph.D. degrees in mechanical engineering from the Massachusetts Institute of Technology (MIT), Cambridge, in 1997 and 2002, respectively.

From 2002 to 2003, he was a Postdoctoral Associate with the Department of Mechanical Engineering, MIT. From 2003 to 2004, he was an Assistant Professor of mechanical engineering with North Dakota State University, Fargo. Since 2005, he has been an Assistant Professor with the Department of Mechanical Engineering, University of Utah, Salt Lake City. He is the author or coauthor of the paper on fingernail sensing, which was published in *Haptics-e: The Electronic Journal of Haptics Research*, in 2006. His current research interests include robotics and control, system dynamics, human–machine interaction, haptics, and bioinspired actuation.

Dr. Mascaro received the Best Paper Award at the 1999 IEEE International Conference on Robotics and Automation for his original work on fingernail sensors, which was published in the IEEE TRANSACTIONS ON ROBOTICS AND AUTOMATION in 2001 and 2004. He is also a member of the American Society of Mechanical Engineers.